Ultramicroscopy 176 (2017) 93–98

Contents lists available at ScienceDirect

Ultramicroscopy

journal homepage: www.elsevier.com/locate/ultramic

The atomic structure of polar and non-polar InGaN quantum wells and the green gap problem

C.J. Humphreys [a,*], J.T. Griffiths [a], F. Tang [a], F. Oehler [b], S.D. Findlay [c], C. Zheng [d], J. Etheridge [e], T.L. Martin [f], P.A.J. Bagot [f], M.P. Moody [f], D. Sutherland [g], P. Dawson [g], S. Schulz [h], S. Zhang [a], W.Y. Fu [a], T. Zhu [a], M.J. Kappers [a], R.A. Oliver [a]

[a] Department of Materials Science and Metallurgy, University of Cambridge, 27 Charles Babbage Road, Cambridge CB3 0FS, UK
[b] CNRS/C2N, Paris Sud University, Route de Nozay, 91460 Marcoussis, France
[c] School of Physics and Astronomy, Monash University, Victoria 3800, Australia
[d] Monash Centre for Electron Microscopy, Monash University, Victoria 3800, Australia
[e] Department of Materials Science and Engineering, Monash University, Victoria 3800, Australia
[f] Department of Materials, University of Oxford, Parks Road, Oxford OX1 3PH, UK
[g] School of Physics and Astronomy, Photon Science Institute, University of Manchester, Manchester M13 9PL, UK
[h] Tyndall National Institute, Lee Maltings Complex, Dyke Parade, Cork, Ireland

ARTICLE INFO

Article history:
Received 18 August 2016
Received in revised form
10 January 2017
Accepted 22 January 2017
Available online 3 February 2017

Keywords:
Gallium nitride
Atomic structure
Quantum wells
Quantitative STEM
Aberration-corrected electron microscopy

ABSTRACT

We have used high resolution transmission electron microscopy (HRTEM), aberration-corrected quantitative scanning transmission electron microscopy (Q-STEM), atom probe tomography (APT) and X-ray diffraction (XRD) to study the atomic structure of (0001) polar and (11-20) non-polar InGaN quantum wells (QWs). This paper provides an overview of the results. Polar (0001) InGaN in QWs is a random alloy, with In replacing Ga randomly. The InGaN QWs have atomic height interface steps, resulting in QW width fluctuations. The electrons are localised at the top QW interface by the built-in electric field and the well-width fluctuations, with a localisation energy of typically 20meV. The holes are localised near the bottom QW interface, by indium fluctuations in the random alloy, with a localisation energy of typically 60meV. On the other hand, the non-polar (11-20) InGaN QWs contain nanometre-scale indium-rich clusters which we suggest localise the carriers and produce longer wavelength (lower energy) emission than from random alloy non-polar InGaN QWs of the same average composition. The reason for the indium-rich clusters in non-polar (11-20) InGaN QWs is not yet clear, but may be connected to the lower QW growth temperature for the (11-20) InGaN QWs compared to the (0001) polar InGaN QWs.

1. Introduction

Bob Sinclair and Nestor Zaluzec have pioneered the use of electron microscopy and analysis to characterise the structure of materials at the nanoscale. High resolution electron microscopy has been central to the research of Sinclair, particularly aberration-corrected transmission electron microscopy. He has utilised high resolution electron microscopy to analyse a wide range of materials and devices, from seminal work on silicide thin-films on silicon [1] to quantum dots in living mice [2].

Zaluzec has developed state-of-the-art instrumentation for electron and X-ray spectroscopy, and analytical electron microscopy. He has recently investigated how aberration-corrected transmission electron microscopes can be re-engineered to improve the sensitivity of spectroscopy in analytical modes. He has studied a wide range of materials, from ground-breaking research on high-T_c superconductors [3] to InGaN quantum wells in light emitting diodes [4].

The present paper reports some of our research on the unusual atomic structure of InGaN quantum wells, which relates to the work of Zaluzec [4] and for which aberration-corrected electron microscopy has been essential.

* Corresponding author.
E-mail addresses: colin.humphreys@msm.cam.ac.uk (C.J. Humphreys), jg641@cam.ac.uk (J.T. Griffiths), ft274@cam.ac.uk (F. Tang), fabrice.oehler@lpn.cnrs.fr (F. Oehler), scott.findlay@monash.edu (S.D. Findlay), changlin.zheng@monash.edu (C. Zheng), joanne.etheridge@mcem.monash.edu (J. Etheridge), tomas.martin@materials.ox.ac.uk (T.L. Martin), paul.bagot@materials.ox.ac.uk (P.A.J. Bagot), michael.moody@materials.ox.ac.uk (M.P. Moody), danny.sutherland@manchester.ac.uk (D. Sutherland), philip.dawson@manchester.ac.uk (P. Dawson), stefan.schulz@tyndall.ie (S. Schulz), siyuan.zhang@mpie.de (S. Zhang), wyfu@hku.hk (W.Y. Fu), mjk30@cam.ac.uk (M.J. Kappers), rao28@cam.ac.uk (R.A. Oliver).

http://dx.doi.org/10.1016/j.ultramic.2017.01.019

2. The surprising success of InGaN quantum wells

The use of InGaN light emitting diodes (LEDs) in solid state lighting and high brightness displays is rapidly increasing [5], and it seems likely that InGaN LEDs will become the dominant form of lighting throughout the world, saving over 10% of electricity globally and 10% of carbon emissions from power stations. At the heart of these LEDs are polar InGaN/GaN quantum wells (QWs) which emit visible light with high internal quantum efficiency (IQE). For example, such blue light emitting LEDs can exhibit IQE values as high as 90% at room temperature [6]. This high efficiency is surprising because the lattice mismatch of GaN on sapphire (the usual substrate in commercial GaN LEDs) is 16%, which leads to a high density of misfit dislocations at the GaN/sapphire interface and to threading dislocations passing through the InGaN QWs with a density of at least $10^8 cm^{-2}$. In other light-emitting semiconductors, such as GaAs, the dislocation density needs to be less than $10^3 cm^{-2}$ to prevent significant loss of light due to the non-radiative recombination of carriers at the dislocations. It is known from cathodoluminescence (CL) studies that dislocations in InGaN are non-radiative recombination centres. Hence a key question is why the efficiency of blue emitting InGaN/GaN LEDs is so high when the dislocation density is so large.

3. The green gap problem in LEDs

White LEDs used for lighting typically use a blue-emitting InGaN/GaN LED covered with a yellow emitting phosphor, the combination of blue and yellow light producing a cool white light. If a warmer white light is desired, a red emitting phosphor is used as well. However, the obvious way to produce white light is to mix red, green and blue LEDs. This would produce even more efficient white light than using a blue LED with phosphors because the Stokes shift energy loss of converting a high energy blue photon to a lower energy yellow or red photon would be avoided, as would efficiency losses in the phosphors themselves. However, we cannot do this efficiently at present due to the "green gap" problem. The experimentally determined external quantum efficiency (EQE) of 400nm (violet) LEDs is very high, over 80%, and for 650nm (red), it is also very high, over 70%, but for green and yellow emission the EQE drops to about 20% [7]. This "Green Gap" has important technological consequences. If one wishes to make white light by mixing red, green and blue LEDs, one red, one blue and three green LEDs are typically required, making such a white light source expensive.

The green gap in nitride LEDs may in part be attributed to internal electric fields due to the large spontaneous and piezoelectric polarisations that produce high fields of $\sim 10^6 Vcm^{-1}$ across the QWs. The active region in nitride LEDs is one or more InGaN QWs sandwiched between the wider bandgap GaN barriers to confine the carriers. The epitaxial InGaN QWs are strained because InGaN has a larger lattice parameter than GaN. Commercial InGaN/GaN QW LEDs are grown in the polar [0001] direction. The strain in an InGaN QW increases as the indium content increases, hence the piezoelectric field across an InGaN QW increases as the indium content increases. This field separates the electrons and holes to opposite sides of the QW, the separation increasing as the indium content increases. Hence the electron-hole wave-function overlap decreases as the indium content increases. This may result in the efficiency of InGaN/GaN green LEDs being less than that of blue LEDs because the decreased electron and hole overlap in green QWs results in increased radiative lifetimes, which in the presence of non-radiative recombination paths can lead to reduced values of the IQE and EQE. The electric field across an InGaN QW can be suppressed by growing the InGaN/GaN QW structure along a non-polar direction. This would be expected to produce green LEDs with high efficiency, hence we have recently explored this and obtained some surprising results.

4. The atomic structure of polar

It was realised as long ago as 1997 that since blue InGaN QWs emitted brilliant light despite having a very high density of dislocations, and since cathodoluminescence showed that dislocations were non-radiative recombination centres in InGaN, there must be some microstructural feature of the InGaN QWs that was localising the carriers and preventing them from moving to the dislocations. There was at the time broad agreement in the GaN scientific community that indium-rich clusters in the InGaN QWs were responsible for localising the carriers [8-16]. Since the bandgap of InN is smaller than that of GaN, indium-rich clusters in an InGaN QW will have a smaller bandgap and hence localise the carriers. The widespread belief in this localisation mechanism was based upon three pieces of scientific evidence. First, high resolution transmission electron microscopy (HRTEM) revealed localised regions of strain contrast about 2nm across which were interpreted as being highly indium rich. This was supported by data from electron energy loss spectroscopy (EELS) [8-16]. Second, photoluminescence (PL) measurements of the temperature dependence of the peak photon energy emitted from an InGaN QW revealed an S-shaped dependence characteristic of carrier localisation [17]. Thirdly, thermodynamic calculations revealed that InGaN was an unstable alloy which would decompose into indium rich and indium poor regions [18]. These three independent pieces of evidence appeared to provide strong scientific support for there being gross indium-rich clusters in InGaN QWs, and this was universally accepted by the scientific community.

In 2003, it was shown that InGaN QWs were extremely sensitive to radiation damage in TEM and that HRTEM images acquired immediately after first irradiating a region of an InGaN QW showed no detectable indium-rich regions [19-21]. The papers further revealed that continued exposure to the electron beam led to the formation of locally strained regions that appeared similar to those previously attributed to indium rich clusters. So it was concluded that the indium-rich clusters observed by many others were due to electron beam damage. This was subsequently supported by multiple research groups by a variety of methods [22-27].

However, InGaN can decompose if there are macrosteps on the growth surface, since indium is incorporated differently at treads and risers of these macrosteps, which leads to compositional growth striations [28]. A recent example of this is atomic-level ordering in InGaN quantum dots in GaN nanowires. This was attributed to a non-flat growth front at vicinal surface facets [29]. In other recent work, indium fluctuations were observed in InGaN/GaN core-shell nanorods, and these were correlated with atomic steps at the GaN/InGaN core-shell interface giving rise to a change in the growth mode from 2D (planar) to 3D (faceted) [30]. Apart from these examples of faceted growth, there is now almost universal acceptance that in (0001) InGaN quantum wells grown by 2D layer-by-layer growth, as in planar LEDs, there are no gross indium-rich clusters.

Galtrey et al [31] used atom probe tomography (APT) not only to confirm that there were no indium-rich clusters in (0001) InGaN QWs but also to demonstrate that InGaN was a random alloy. APT was also used to show that an electron beam in TEM can create In-rich clusters in InGaN [32]. These results appeared to conflict with the thermodynamic calculations that showed that InGaN should decompose into indium rich and indium poor regions at the growth temperature used [18]. However, these

calculations had been performed for bulk InGaN, and, in a paper that had been somewhat overlooked, Karpov had shown that for strained InGaN QWs, the strain suppressed the decomposition and that blue and green emitting InGaN QWs should be stable at the growth temperatures used [33]. So the thermodynamics now agreed with the HRTEM and APT results. However, the PL results clearly showed that the carriers in InGaN were localised. If there were no indium-rich clusters, then what was the localisation mechanism?

HRTEM was used to show that the lower GaN/InGaN interface appeared to be atomically smooth, but that the upper InGaN/GaN interface had atomic height interface steps, typically about 5nm across [34]. This was later confirmed using APT [35]. The interface steps resulted in QW width fluctuations on an atomic scale. A key question was whether such well width fluctuations and random indium fluctuations played any role in localising the carriers in the InGaN QWs.

4.1. Localisation mechanisms in InGaN

The above atomic structure results from HRTEM and APT were fed into quantum mechanical calculations independently by Watson-Parris et al. using an effective mass treatment [36], and Schulz et al. using an atomistic tight binding model [37]. They both found that the electrons and holes were localised by different mechanisms. The electrons were localised near the top QW interface by the built-in electric field and well width fluctuations, whereas the holes were localised near the bottom QW interface by the random In fluctuations, in regions of higher In concentrations. The localisation energy of the holes was typically about 60meV and of the electrons about 20meV. The large PL linewidth observed from InGaN was found to be mainly due to the fluctuations in the localisation energies of the holes. Schulz et al. [37] also found that these localisation energies of the electrons and holes in the InGaN QWs are much higher than the electron/hole Coulomb interaction energy, which is relatively weak because of the spatial separation of the electrons and holes due to the built-in potential. Hence the electrons and holes essentially act as independent carriers in the QWs and not as excitons. It is worth noting that this detailed understanding of electrons and holes in polar InGaN QWs is based upon observations of the atomic structure of the wells using HRTEM and APT, these experimental results then being input as data into theoretical calculations. However, in non-polar QWs there is no electric field across the QWs, and the electrons and holes are not spatially separated. Hence we now discuss the structure and origin of localisation in non-polar (11-20) InGaN QWs.

5. Comparing polar and non-polar InGaN QWs

5.1. Sample details

Four non-polar a-plane (11-20) samples with five InGaN/GaN QWs were grown by metal organic vapour phase epitaxy (MOVPE) in a Thomas Swan 6 × 2in close coupled showerhead reactor (see Fig. 1). Trimethylgallium (TMG), trimethylindium (TMI), and ammonia were used as the precursors, with hydrogen as the carrier gas, for the growth of the GaN epilayer, and nitrogen for the growth of the InGaN QWs and GaN barrier layers. The samples were grown on ammonothermal GaN substrates to reduce the high density of stacking faults and dislocations which would otherwise have formed in these non-polar samples. The substrates had a miscut of 0.3 ± 0.20° towards [0001]. An 800nm non-intentionally doped GaN epilayer was grown directly on the substrate. Five period InGaN/GaN QWs were grown at 300Torr in a constant ammonia flow of 446mmol/min. The InGaN QWs were grown for 160s with a TMI flow of 14.5μmol/min and a TMG flow of 4.5μmol/min. The indium composition in the QWs was varied by changes in the growth temperature between 705 and 690°C, to give an indium content in all four samples varying from 8% to 21%, as measured by X-ray diffraction. Following the growth of each InGaN QW, a 1nm GaN protective cap layer was grown at the same temperature and TMG flow rate as during the InGaN growth. The GaN barrier growth continued during the temperature ramp up to 860°C over 90 seconds at which point the TMG flow rate was increased to 73.2μmol/min for the remainder of the barrier. Further growth details are given in ref. [38].

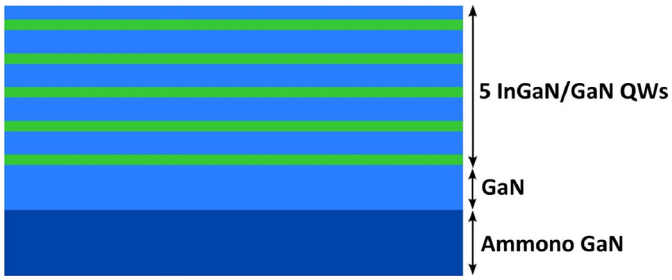

Fig. 1. Schematic diagram of the structure of the non-polar specimens. Five InGaN QWs with GaN barriers were grown by MOVPE on an a-plane ammonothermal GaN substrate. The thickness of the GaN layer grown on the Ammono substrate was 900nm. The nominal thickness for the QWs and barriers were 2.0nm and 6.0nm respectively.

For comparison, four polar samples were grown on (0001) sapphire with a miscut of 0.25 ± 0.10° towards [11-20]. A 5μm thick GaN pseudo-substrate was grown following a two-step approach as described by Das Bakshi et al. [39], this was followed by the growth of 400nm of non-intentionally doped GaN. The QWs were grown at 300Torr in a constant ammonia flow of 446mmol/min. The InGaN QWs were grown for 216s with a TMI flow of 14.5μmol/min and a TMG flow of 4.5μmol/min. The indium composition between the samples was varied by changes in the growth temperature from 779, 771, 754, and 744°C. The barriers were grown under the same conditions previously used for the non-polar samples.

5.2. Results: the apparent disagreement of theory and experiment for non-polar InGaN QWs

The $In_x Ga_{1-x} N$ indium composition, defined in this study as the group-III alloy fraction (x), was quantified using X-ray diffraction (XRD). XRD is a rapid, non-destructive and widely used technique to measure the indium composition in InGaN QWs. High resolution XRD was performed on a Philips X'pert MRD diffractometer with a 4-bounce monochromator and a triple axis analyser. The QW widths and lattice parameters were determined by $\omega - 2\theta$ scans following the approach of Vickers et al [40] for the polar samples and its adaptation to non-polar orientations [41]. XRD does not reveal variations in the composition between QWs or within the QW, but it can provide information on the average composition for the QWs [38,42].

Fig. 2 shows experimental points for the PL peak emission wavelength from the InGaN QWs as a function of the indium composition, as measured by XRD, for the polar and (11-20) non-polar structures. We have also calculated the change in emission wavelength as a function of the indium composition using a commercially available package for the simulation of semiconductor nanostructures, nextnano3, which assumes that the InGaN in the QWs is a uniform alloy.

While the simulated emission wavelength of the polar (0001) InGaN QWs agrees reasonably with the observed results, for the

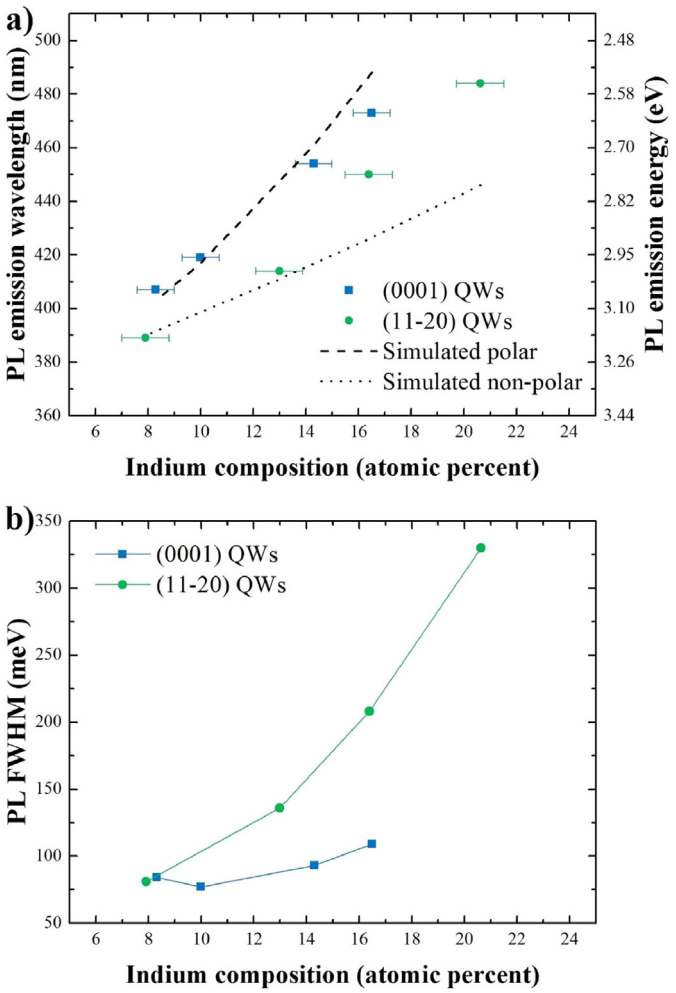

Fig. 2. (a) PL emission wavelength at 10K as a function of the indium content of InGaN QWs measured by XRD for (0001) polar and (11-20) non-polar QWs, experimental points and simulated curves. (b) FWHM of the PL emission spectrum as a function of the indium content.

non-polar (11-20) InGaN QWs the experiment and theory do not agree, particularly at longer wavelengths. It would seem that either the structural assumptions used in the theory are wrong, or the indium content measured by XRD is wrong for the non-polar samples. In addition, we note from Fig. 2 that the PL emission spectrum is much broader for the non-polar specimens than for the polar. Again, this is an unexpected result and it is not obvious why this should be the case. These surprising and unexpected results drove us to perform a more detailed characterisation of the atomic structure of our non-polar InGaN QWs.

5.3. *Results from APT and aberration-corrected quantitative-STEM*

Fig. 3 shows an APT atom map of the indium distribution in a non-polar (11-20) InGaN QW. Visually, some indium-rich clusters are apparent. To quantitatively study the indium distribution, a frequency distribution analysis of the indium distribution was performed (Fig. 4). Analysis was performed with histogram bin sizes ranging from 25 to 200 atoms in increments of 25 atoms, corresponding to volumes with linear dimensions ranging from 1.2 to 2.4nm. (For example, taking into account the detection efficiency of the atom probe gives the size of a 100 atom bin as $1.55 \times 1.55 \times 1.55\text{nm}^3$ [43].) The experimental distribution of indium atoms exhibits significant deviations when compared with a random binomial distribution. Evidence of a non-random

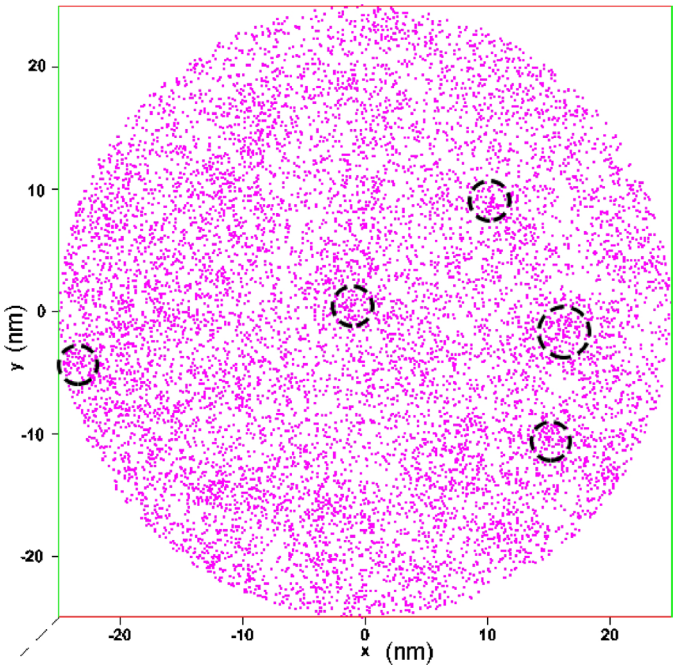

Fig. 3. APT atom map of the indium distribution in a non-polar (11-20) InGaN QW. Note the indium-rich clusters. The map is a 2D in-plane projection, (11-20) plane, of all indium atoms in the first QW, integrated over the thickness of the well.

distribution requires a *p*-value less than 0.05 [44]. A χ^2 analysis of the data in Figs. 4 and 5 yields a *p*-value less than 0.001, indicating no statistical correlation between the experimental data and a random distribution [45].

The APT result, that there are indium-rich clusters in non-polar (11-20) InGaN QWs, was unexpected and contrary to the observations in polar InGaN QWs and we therefore decided to investigate further the atomic structure of these non-polar QWs using quantitative scanning transmission electron microscopy (Q-STEM) in an FEI Titan^3 80–300keV Schottky field emission gun TEM fitted with spherical aberration correctors on the probe and image-forming lenses at the electron microscope facility at Monash University. Further details are given in ref. [38]. We used Q-STEM because InGaN is sensitive to radiation damage in an electron microscope [19-21]. Q-STEM can provide high spatial resolution and chemical sensitivity with a lower electron dose than energy dispersive X-ray spectroscopy (EDS) or electron energy loss spectroscopy (EELS). As previously reported by Rosenauer et al [46], we found no evidence for the formation of indium-rich regions, or other observable damage induced by the electron beam, for the low doses we used in Q-STEM.

For quantitative compositional analysis of our HAADF-STEM images, theoretical HAADF-STEM intensities were simulated for comparison using a frozen phonon multislice model following the approach of Rosenauer et al [46] using electron image simulation software adapted from the Melbourne μSTEM code [47]. Image intensity calculations were performed for indium fractions from 0 to 0.24 in steps of 0.04, up to a maximum thickness of 130nm. The calculations assumed the same incident electron energy, probe convergence and detector response as used in the experiment. Comparison between the simulated and experimental intensities, as described in ref. [37], was used to produce an indium composition image, as shown in Fig. 5. The distribution of indium in each of the five QWs is revealed. The HAADF-STEM results show variations in projected In concentration, and strain contrast, which would be expected if clustering occurs in this (11-20) non-polar sample. Because the HAADF-STEM image is a projection of the structure, these indium-rich regions could be indium-rich nano-

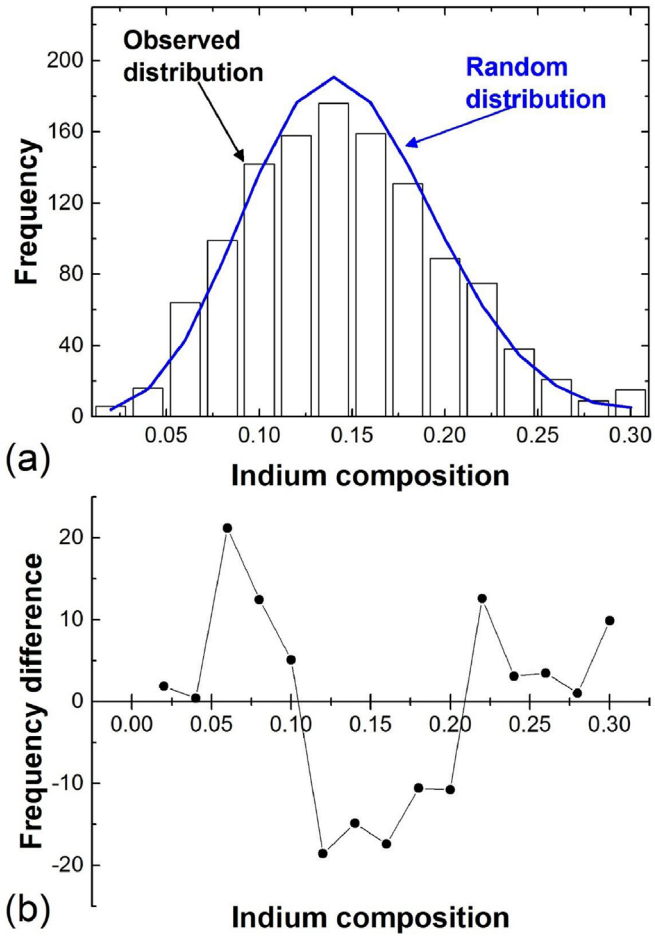

Fig. 4. (a) Frequency distribution analysis of the indium content in the first non-polar (11-20) InGaN QW using a bin size of 50 atoms. (b) The frequency difference between the experimental data and a binomial (random) distribution. The frequency difference data have a *p*-value of less than 0.001, indicating a clear deviation from a random distribution of indium atoms.

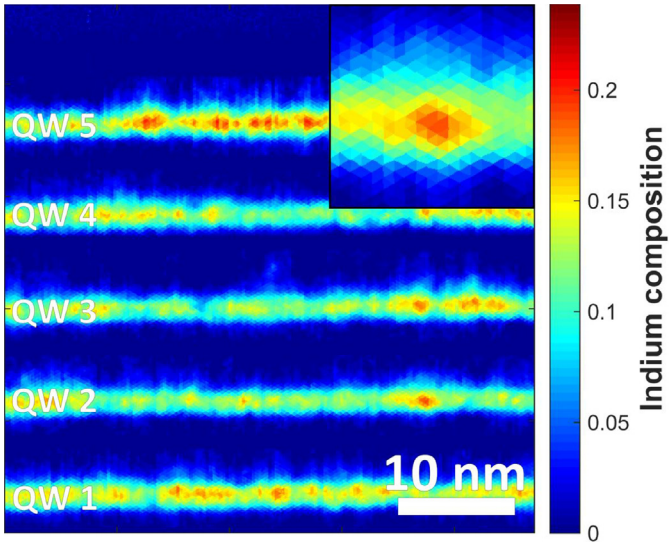

Fig. 5. The distribution of indium in each of the non-polar (11-20) InGaN QWs. Indium-rich regions are clear (see also the inset). Specimen thickness 80nm. Zone axis orientation [0001].

wires running along the electron beam direction, but the APT result confirms that they are, in fact, nm-scale In-rich clusters. The size of these clusters agrees with those seen in the APT images. Since our findings, quantitative-STEM has also been applied to reveal locally indium rich regions on non-polar m-plane (1-100) sidewalls in InGaN core-shell nanorods [48].

5.4. Discussion of the non-polar (11-20) InGaN QW results

Since the bandgap of InN is less than that of GaN, it is suggested that indium-rich clusters in the non-polar (11-20) InGaN QWs will localise the carriers and produce longer wavelength (lower energy) emission than from a random InGaN alloy of the same average composition. This may explain the apparent discrepancy between theory and experiment for non-polar (11-20) InGaN in Fig. 2(a), in which the theory is for a random alloy. The indium-rich clusters in non-polar (11-20) InGaN QWs may also explain the broad spectral line widths from this material shown in Fig. 2(b).

The average composition measured by APT and Q-STEM agreed quantitatively with XRD measurements, but only APT and Q-STEM had the resolution to reveal the indium-rich clusters in non-polar (11-20) InGaN QWs. The reason for the clustering is not yet clear, but may be due to the lower QW growth temperature for the (11-20) InGaN QWs compared to the (0001) polar InGaN QWs.

6. Conclusions

For polar (0001) InGaN QWs, the calculated wavelength as a function of the In content is in agreement with theory, assuming InGaN to be a random alloy. For non-polar (11-20) InGaN QWs, the calculated wavelength apparently disagrees with experiment. However aberration-corrected Q-STEM and APT reveal that in non-polar (11-20) InGaN QWs there are indium-rich clusters, instead of InGaN being a random alloy. When these large indium fluctuations are taken into account there is agreement of theory and experiment.

Aberration-corrected electron microscopy has been an essential technique to solve the problems reported in this paper. Bob Sinclair and Nestor Zaluzec have made major contributions to this technique and its applications and we have built upon their outstanding research.

Acknowledgements

We thank the UK Engineering and Physical Sciences Research Council for their support (grants EP/J001627/1, EP/I01259/1, and EP/J003603/1).

References

[1] R. Beyers, R. Sinclair, J. Appl. Phys. 57 (1985) 5240.
[2] M.L. Schipper, G. Iyer, A.L. Koh, Z. Cheng, Y Ebenstein, A. Aharoni, S. Keren, L. A. Bentolila, J.Q. Li, J.H. Rao, X.Y. Chen, U. Banin, A.M. Wu, R. Sinclair, S. Weiss, S.S. Gambhir, Small 5 (2009) 126.
[3] J.W. Ekin, A.I. Braginski, A.J. Panson, M.A. Janocko, D.W. Capone, N.J. Zaluzec, B. Flandermeyer, O.F. de Lima, M. Hong, J. Kwo, S.H. Liou, J. Appl. Phys. 62 (1987) 4821.
[4] I.H. Wildeson, R. Colby, D.A. Ewoldt, Z. Liang, D.N. Zakharov, N.J. Zaluzec, R. E. Garcia, E.A. Stach, T.D. Sands, J. Appl. Phys. (2010) 044303.
[5] C.J. Humphreys, MRS Bull. 33 (2011) 459.
[6] T. Sano, T. Doi, S.A. Inada, T. Sugiyama, Y. Honda, H. Amano, T. Yoshino, Jpn. J. Appl. Phys. 52 (Part 1) (2013) 08JK09.
[7] M. Auf der Maur, A. Pecchia, G. Penazzi, W. Rodrigues, A. Di Carlo, Phys. Rev. Lett. (2016) 027401.
[8] S. Chichibu, K. Wada, S. Nakamura, Appl. Phys. Lett. 71 (1997) 2346.
[9] C. Kisielowski, Z. Liliental-Weber, S. Nakamura, Jpn. J. Appl. Phys. 36 (Part I) (1997) 6932.
[10] Y. Narukawa, Y. Kawakami, M. Funato, M. Fujita, S. Fujita, S. Nakamura, Appl. Phys. Lett. 70 (1997) 981.
[11] P. Ruterana, S. Kret, A. Vivet, G. Maciejewski, P. Dluzewski, J. Appl. Phys. 91

(2015) 8979.
[12] S. Srinivasan, F. Bertram, A. Bell, F.A. Ponce, S. Tanaka, H. Omiya, Y. Nakagawa, Appl. Phys. Lett. 80 (2002) 550.
[13] F.A. Ponce, S. Srinivasen, A. Bell, L. Geng, R. Liu, M. Stevens, J. Cai, H. Omiya, H. Marui, S. Tanaka, Phys. Status Solidi B 240 (2003) 273.
[14] H.K. Cho, J.Y. Lee1, N. Sharma, C.J. Humphreys, G.M. Yang, C.S. Kim, J.H. Song, P. W. Yu, Appl. Phys. Lett. 79 (2001) 2594.
[15] D. Gerthsen, E. Hahn, B. Neubauer, A. Rosenauer, O. Schön, M. Heuken, A. Rizzi, Phys. Status Solidi A 177 (2000) 145.
[16] H. Lakner, G. Brockt, C. Mendorf, A. Radefeld, F. Scholz, V. Härle, J. Off, A. Sohmer, J. Electron. Mater. 26 (1997) 1103.
[17] Y.H. Cho, G.H. Gainer, A.J. Fischer, J.J. Song, S. Keller, U.K. Mishra, S.P. DenBaars, Appl. Phys. Lett. 73 (1998) 1370.
[18] I. Ho, G.B. Stringfellow, Appl. Phys. Lett. 69 (1996) 2701.
[19] T.M. Smeeton, M.J. Kappers, J.S. Barnard, M.E. Vickers, C.J. Humphreys, Phys. Status Solidi B 204 (2003) 297.
[20] J.P. O'Neill, I.M. Ross, A.G. Cullis, T. Wang, P.J. Parbrook, Appl. Phys. Lett. 83 (2003) 1965.
[21] T.M. Smeeton, M.J. Kappers, J.S. Barnard, M.E. Vickers, C.J. Humphreys, Appl. Phys. Lett. 83 (2003) 5419.
[22] T. Schulz, T. Remmele, T. Markurt, M. Korytov, M. Albrecht, J. Appl. Phys. (2012) 033106.
[23] T. Schulz, A. Duff, T. Remmele, M. Korytov, T. Markurt, M. Albrecht, L. Lymperakis, J. Neugebauer, C. Chèze, C. Skierbiszewski, J. Appl. Phys. (2014) 033113.
[24] X.J. Chen, J.S. Hwang, G. Perillat-Merceroz, S. Landis, B. Martin, D. Le Si Dang, J. Eymery, C. Durand, J. Cryst. Growth 322 (2011) 15.
[25] D. Salomon, A. Dussaigne, M. Lafossas, C. Durand, C. Bougerol, P. Ferret, J. Eymery, Nanoscale Res. Lett. 8 (2013) 61.
[26] L. Rigutti, I. Blum, D. Shinde, D. Hernández-Maldonado, W. Lefebvre, J. Houard, F. Vurpillot, A. Vella, M. Tchernycheva, C. Durand, J. Eymery, B. Deconihout, Nano Lett. 14 (2014) 107.
[27] T. Walther, H. Amari, I.M. Ross, T. Wang, A.G. Cullis, J. Mater. Science 48 (2013) 2883.
[28] M. Kryśko, G. Franssen, T. Suski, M. Albrecht, B. Łucznik, I. Grzegory, S. Krukowski, R. Czernecki, S. Grzanka, I. Makarowa, M. Leszczyński, P. Perlin, Appl. Phys. Lett. (2007) 211904.
[29] S.Y. Woo, M. Bugnet, H.P.T. Nguyen, Z. Mi, G.A. Botton, Nano Lett. 15 (2015) 6413.
[30] P.-M. Coulon, S. Hosseini Vajargah, A. Bao, P.R. Edwards, E.D. Le Boulbar, I. Gîrgel, R.W. Martin, C.J. Humphreys, R.A. Oliver, D.W.E. Allsopp, P.A. Shields, Cryst. Growth Des. 17 (2017) 474.
[31] M.J. Galtrey, R.A. Oliver, M.J. Kappers, C.J. Humphreys, P. Clifton, D. Lawson, D. Saxey, A. Cerezo, J. Appl. Phys. (2008) 013524.
[32] S.E. Bennett, D.W. Saxey, M.J. Kappers, J.S. Barnard, C.J. Humphreys, G.D. W. Smith, R.A. Oliver, Appl. Phys. Lett. (2011) 021906.
[33] S.Y. Karpov, MRS Internet J. Nitride Semicond. Res. 3 (1998) 16.
[34] D.M. Graham, A. Soltani-Vala, P. Dawson, M.J. Godfrey, T.M. Smeeton, J. S. Barnard, M.J. Kappers, C.J. Humphreys, E.J. Thrush, J. Appl. Phys. (2005) 103508.
[35] M.J. Galtrey, R.A. Oliver, M.J. Kappers, C.J. Humphreys, P. Clifton, D. Lawson, D. Saxey, A. Cerezo, J. Appl. Phys. (2008) 013524.
[36] D. Watson-Parris, M.J. Godfrey, P. Dawson, R.A. Oliver, M.J. Galtrey, M. J. Kappers, C.J. Humphreys, Phys. Rev. B (2011) 115321.
[37] S. Schulz, M.A. Caro, C. Coughlan, E.P. O'Reilly, Phys. Rev. B (2015) 035439.
[38] J.T. Griffiths, F. Oehler, F. Tang, S. Zhang, W.Y. Fu, T. Zhu, S.D. Findlay, C. Zheng, J. Etheridge, T.L. Martin, P.A.J. Bagot, M.P. Moody, D. Sutherland, P. Dawson, M. J. Kappers, C.J. Humphreys, R.A. Oliver, J. Appl. Phys. (2016) 175703.
[39] S. Das Bakshi, J. Sumner, M.J. Kappers, R.A. Oliver, J. Cryst. Growth 311 (2009) 232.
[40] M.E. Vickers, M.J. Kappers, T.M. Smeeton, E.J. Thrush, J.S. Barnard, C. J. Humphreys, J. Appl. Phys. 94 (2003) 1565.
[41] M.E. Vickers, J.L. Hollander, C. McAleese, M.J. Kappers, M.A. Moram, C. J. Humphreys, J. Appl. Phys. (2012) 043502.
[42] H. Amari, I.M. Ross, T. Wang, T. Walther, Phys. Status Solidi C 9 (2012) 546.
[43] M.J. Galtrey, R.A. Oliver, M.J. Kappers, C.J. Humphreys, P.H. Clifton, A. Cerezo, G. D.W. Smith, Appl. Phys. Lett. (2007) 176101.
[44] M.J. Galtrey, R.A. Oliver, M.J. Kappers, C.M. McAleese, D. Zhu, C.J. Humphreys, P.H. Clifton, D.J. Larson, A. Cerezo, Phys. Status Solidi B 245 (2008) 861.
[45] F. Tang, T. Zhu, F. Oehler, W.Y. Fu, J.T. Griffiths, F.C.-P. Massabuau, M.J. Kappers, T.L. Martin, P.A.J. Bagot, M.P. Moody, R.A. Oliver, Appl. Phys. Lett. (2015) 072104.
[46] A. Rosenauer, T. Mehrtens, K. Müller, K. Gries, M. Schowalter, P.V. Satyam, S. Bley, C. Tessarek, D. Hommel, K. Sebald, M. Seyfried, J. Gutowski, A. Avramescu, K. Engl, S. Lutgen, Ultramicroscopy 111 (2011) 1316.
[47] L.J. Allen, A.J. D'Alfonso, S.D. Findlay, Ultramicroscopy 151 (2015) 11.
[48] M. Müller, P. Veit, F.F. Krause, T. Schimpke, S. Metzner, F. Bertram, T. Mehrtens, K. Müller-Caspary, A. Avramescu, M. Strassburg, A. Rosenauer, J. Christen, Nano Lett. 16 (2016) 5340.